Motile dissenters disrupt the flocking of active granular matter

Pradip K. Bera and A. K. Sood*
Department of Physics, Indian Institute of Science, Bangalore 560012, India

(Received 18 February 2020; accepted 13 May 2020; published 27 May 2020)

We report flocking in the dry active granular matter of millimeter-sized two-step-tapered rods without an intervening medium. The system undergoes the flocking phase transition at a threshold area fraction of ∼0.12 having high orientational correlations between the particles. However, the one-step-tapered rods do not flock and are used as the motile dissenters in the flock-forming granular matter. At the critical fraction of dissenters of ∼0.3, the flocking order of the system gets completely destroyed. The variance of the system's order parameter shows a maximum near the dissenter fraction $f \sim 0.05$, suggesting a finite-size crossover between the ordered and disordered phases. Our experiments bring out the disruption of the cooperative behavior in heterogeneous active systems with possible implications in real-life examples.

DOI: 10.1103/PhysRevE.101.052615

I. INTRODUCTION

The effect of static defects or motile nonaligning agents (called dissenters [1]) on the flocking or other collective motions of a group is a subject of recent interest in model systems and simulations [2–16]. Disordered environment in the form of physical obstacles is found to alter the group's motion dramatically by bringing spatial heterogeneity into the system. Laboratory experiments using colloidal rollers show that the obstacle critical fraction to destroy the flocking increases monotonically with the roller packing fraction. The ratio of the critical obstacle packing fraction to the roller packing fraction was rather high (4:1) [6]. In comparison, the effect of nonaligning self-propelled particles on the global polar order has been studied only numerically [1,17]. Studying an agent-based model of finite swarms with local aligning and cohesive interactions between neighbors and a subpopulation of nonaligning agents (called motile dissenters that do not align with their neighbours and do not have a defined internal preferred velocity) within the group, Copenhagen *et al.* [17] have shown that at the dissenter critical fraction of ∼0.5 the system goes to the nonswarming state. Later, focusing on the case where the self-propelled agents only experience repulsive interactions due to volume exclusion, in addition to alignment, Yllanes *et al.* [1] have reported that even a small concentration of dissenters (∼0.1) disrupts the flocking state completely. However, to date, there are no experiments to study the role of dissenters on the flocking behavior, a motivation for our present study.

We have used two types of brass particles having different degrees of polarity (Fig. 1). Our experimental observations are as follows: (i) Flocking in a granular medium of two-step-tapered polar active agents (called aligners) is observed above a certain area fraction without any intervening medium. (ii) One-step-tapered polar active agents (called dissenters) do not flock even at a very high area fraction. (iii) The mixed systems of flock-forming aligners and dissenter particles show flocking with a low fraction of dissenters. However, above a critical dissenters' fraction, the mixed system does not flock, similar to the simulation results [1,17]. We quantify orientational correlations and other measures as the fraction of dissenters is increased.

II. EXPERIMENTAL DETAILS

Our active granular material is a collection of macroscopic polar brass rods vibrated vertically by a magnetic shaker (LDS V406-PA100E). The aligner rods are 4.5 mm long (denoted by L_a), with the diameter tapered in two steps from 1.1 mm at the thick end to 0.7 mm at the thin end. On the other hand, the dissenter rods are 3.5 mm long, with the diameter tapered in one step from 1.1 mm at the thick end to 0.7 mm at the thin end. Our monolayer of rods is confined in the 1.2-mm gap between the flower-shaped experimental cell and its top glass lid (see Supplemental Material [18] for details about the setup calibration). We keep the shaker oscillation amplitude ($\mathcal{A} = 0.025$ mm) and frequency ($n = 200$ Hz) fixed during our experiments. The nondimensional shaking strength $[(2\pi n)^2\mathcal{A}/g$, where g is gravity] is 4.0 (also measured by the two orthogonally attached MPU-6050 accelerometers). Both types of rods imitate self-propulsion by transducing the vertical vibrations into horizontal motion, in the tail-to-head direction [19–22]. A Redlake MotionPro X3 camera is used to capture images at 30 fps (frames per second) during studies with a single particle and at 1 fps during studies with the collection of particles. Fiji (ImageJ) is used for image analysis [23] (see Supplemental Material [18] for details).

III. RESULTS

The aligner and the dissenter are polar particles with shape asymmetry and hence are self-propelling due to vertical vibrations of the platform. Figure 1 shows the single-particle dynamics captured at 30 fps, of the aligner and the dissenter, present alone in the cell (Supplemental Material [18], Movies

*asood@iisc.ac.in

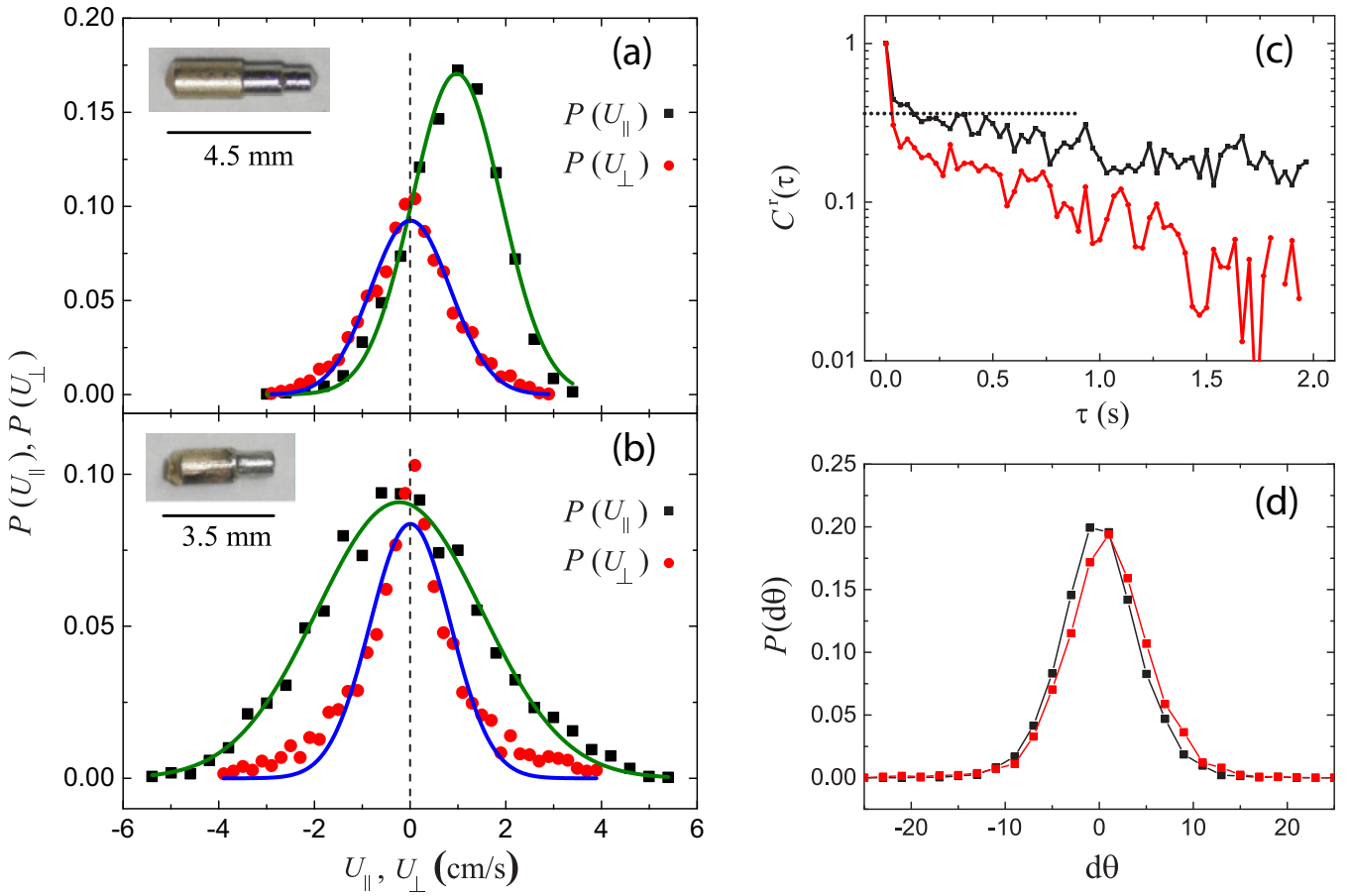

FIG. 1. The single particle in the cell. Distributions of $U_\parallel$ and $U_\perp$ (velocity components along and orthogonal to the polarity direction, respectively) (a) of the two-step-tapered polar active rod, called the aligner, and (b) of the one-step-tapered polar active rod, called the dissenter, are shown. The respective rod images are shown. Solid curves are Gaussian fits with peak positions of ∼1.0 and 0.0 cm/s in panel (a) and ∼−0.2 cm/s (∼resolution limit) and ∼0.0 cm/s in panel (b). Dotted lines represent zero velocity. (c) Rotational autocorrelation functions $[C^r(\tau)]$ vs the time gap (τ). (d) Distributions of the angular displacement ($d\theta$, measured with a time gap of 0.03 s) for the aligner (black symbols) and for the dissenter (red symbols) are shown. The dotted line in panel (c) is at $C^r(\tau) = 1/e$. The shaking strength $\Gamma = 4$ and the shaking frequency $n = 200$ Hz are fixed during our study.

S2 and Movies S3, respectively). Velocity components $U_\parallel$ and $U_\perp$ are calculated by taking the projection of the laboratory frame velocity parallel to the particle polarity direction and orthogonal to the polarity direction, respectively. The statistical anisotropy of the dynamics is evident from the probability distributions of $U_\parallel$ and $U_\perp$ for both the particles [Figs. 1(a) and 1(b)], which show a much greater dispersion along the rod axis direction than transverse to it. For the aligner, the $U_\parallel$ component shows a maximum in the probability distribution $P(U_\parallel)$ at ∼1 cm/s, whereas $P(U_\perp)$ has a peak close to zero. For the dissenter, $P(U_\parallel)$ shows a peak at ∼−0.2 cm/s, close to the resolution limit, whereas $P(U_\perp)$ is peaked close to zero. Both velocity components of aligners and dissenters show Gaussian behavior. Using the orientation $[\theta(t)]$ of the particle polarity direction with respect to the laboratory frame x axis at time t, we calculate the rotational autocorrelation function $C^r(\tau) = \langle \cos[\theta(t+\tau) - \theta(t)] \rangle_t$ for each particle, which is a measure of the rotational noise in the particle motion [Fig. 1(c)]. The very short autocorrelation time of the dissenter (∼0.03 s) implies a very short persistent length. As this correlation time is at the limit of inverse of the frame rate to capture the images, we cannot measure the directed motion of the dissenters precisely and hence the $P(U_\parallel)$ is centered close to the origin. On the other hand, the aligner shows persistent motion with large correlation time (∼0.50 s) and hence the $P(U_\parallel)$ peaks at finite $U_\parallel$. The angular displacements of both the particles (measured over the time interval of 0.03 s) are similar as shown in Fig. 1(d).

Now we disperse the required number of particles in the clean cell and keep the shaker on for 500 s to observe the onset of the flocking transition over time (captured at 1 fps). We repeat this procedure three times with a given set of particles to get good statistical estimations. We first present the collective behavior of only aligners and the collective behavior of only dissenters before presenting the effect of dissenters on the flocking transition.

The collective behavior of the system with only aligners (Supplemental Material [18], Fig. S3 and Movies S4, S5, and S6) is markedly different from that of the system with only dissenters (Supplemental Material [18], Fig. S4 and Movies S7 and S8). At low area fraction $\phi = 0.07$ (ϕ = area covered by the two-dimensional projections of the rods/flower area), aligners show a completely isotropic disordered state. Above a threshold area fraction ($\phi = 0.12$), they form a dynamically

steady flock where most of the rods are aligned along the flocking direction. We quantify (following Ref. [24]) the flocking order for each time frame by resolving the in-plane rod's orientation $\mathbf{n}_i$ into local polar-coordinate components, with the coordinate center located at the flower center, and define $(\mathbf{n}_i \cdot \mathbf{r}_i, \mathbf{n}_i \times \mathbf{r}_i) \equiv \mathbf{P}_i$, where $\mathbf{r}_i$ is the unit radial position vector of the ith particle. For each image frame, we then calculate $P \equiv |\langle \mathbf{P}_i \rangle|$, averaged over all particles. Figure 2(a) shows the growth kinetics of the measured flocking order parameter $[P(t)]$ for the system having only aligners for three area fractions. For $\phi = 0.07$, the system shows a completely isotropic disordered state with $P(t)$ fluctuating near zero, implying disordered state. For $\phi = 0.20$ and 0.30, aligners form a dynamically stable flock within 300 s. The order parameter grows from a random configuration and reaches a steady saturation value close to 1. The average steady-state order parameter ($\langle P \rangle$) is calculated by taking an average of P over the steady-state time frames and then over the three repeated experiments for each ϕ [Fig. 2(b)]. The error bar is the standard deviation in $\langle P \rangle$ over three repeated experiments for the same ϕ. The same calculation strategy is adopted for all $\langle P \rangle$ presented in the subsequent plots. For all the area fractions below 0.13, aligners do not form a dynamically stable flock. Aligners form a dynamically stable flock for the area fractions $0.13 \leqslant \phi \leqslant 0.40$. The smooth variation in order parameter above $\phi = 0.12$ is due to the finite system size effects as the discontinuous flocking transition is observed in the finite but larger system sizes in simulations [25]. For $0.40 < \phi \leqslant 0.70$, the randomly running active matter condensates to a large single cluster of particles and eventually goes to a dynamically jammed state [26]. For $\phi > 0.70$, we observe spatially restricted motion. The condensation and the dynamical jamming are not pursued in this work. We now explore how the orientational correlation function grows as ϕ increases. In Fig. 2(c) we plot the average steady-state orientational correlation function $G(r) = \langle \mathbf{P}_i(0) \cdot \mathbf{P}_j(r) \rangle_{\text{all pairs}}$, a measure of the probability that two rods separated by distance r are pointing in the same direction, and the data is averaged over various pairs in the steady-state frames and in the three repeated experiments. We observe that above $\phi = 0.12$ the system shows long-range correlation. On the other hand, systems with only dissenters do not show flocking up to the highest volume fraction ($\phi = 0.78$). The order parameter $P(t)$ is low [<0.1, see Supplemental Material [18], Fig. S4(e)]. The rotational autocorrelation function (averaged over all the dissenters) $\langle C^{\text{r}}(\tau) \rangle$ decays fast for $\phi < 0.70$, but for $\phi = 0.78$ the particles have spatially restricted motion and hence the $\langle C^{\text{r}}(\tau) \rangle$ retains the high value up to large delay times [Supplemental Material [18], Fig. S4(f) and Movie S8].

We next discuss the effects of dissenters on the flocking. Figure 3 broadly summarizes our experimental findings with the aligner-dissenter mixed system. In the mixed system, the area fraction of aligners and the area fraction of dissenters are denoted by ϕ_{a} and ϕ_{d}, respectively ($\phi = \phi_{\text{a}} + \phi_{\text{d}}$). The trapping and sorting study with these active particles (at low ϕ) and having a trap in the cell is reported elsewhere [22]. At first, to see the effect of dissenters on the flocking behavior of aligners, dissenters are added with an increasing number to increase the total ϕ, keeping the aligners' area fraction constant ($\phi_{\text{a}} = 0.28$), and the mixture is dispersed in the cell

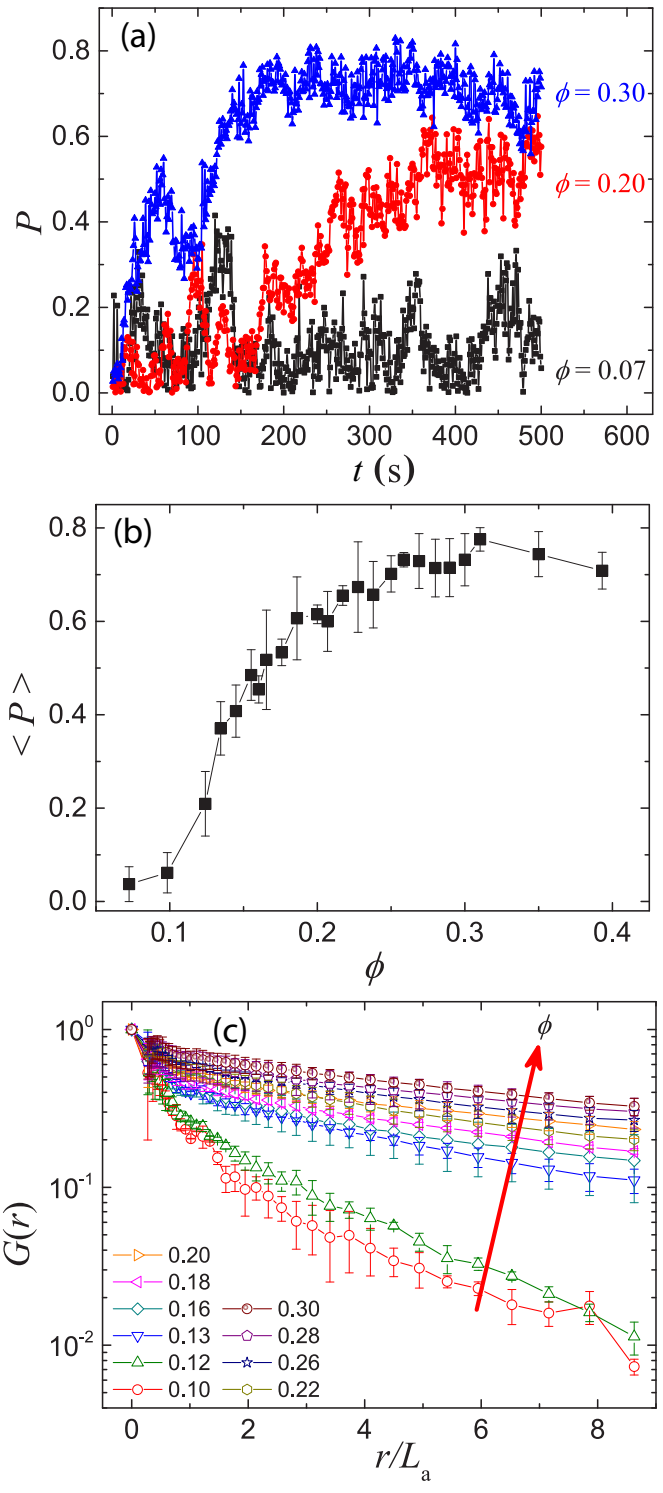

FIG. 2. The system with only aligners. The error bar with each data point represents the standard deviation of the quantity in three repeated experiments. (a) The flocking order parameter $[P(t)]$ vs time (t) is shown for three different area fractions (ϕ). (b) The average steady-state value of $P(t)$ ($\langle P \rangle$, averaged considering steady-state frames and then over the three repeated experiments) is plotted against ϕ. (c) The average orientational correlation function $[G(r)]$ vs the interparticle separation (r/L_{a}, where L_{a} is aligner's length) is plotted for different ϕ. For the given ϕ and r, $G(r)$ is averaged over satisfying pairs in the steady-state frames and then over the three repeated experiments. The red arrow is towards increasing ϕ.

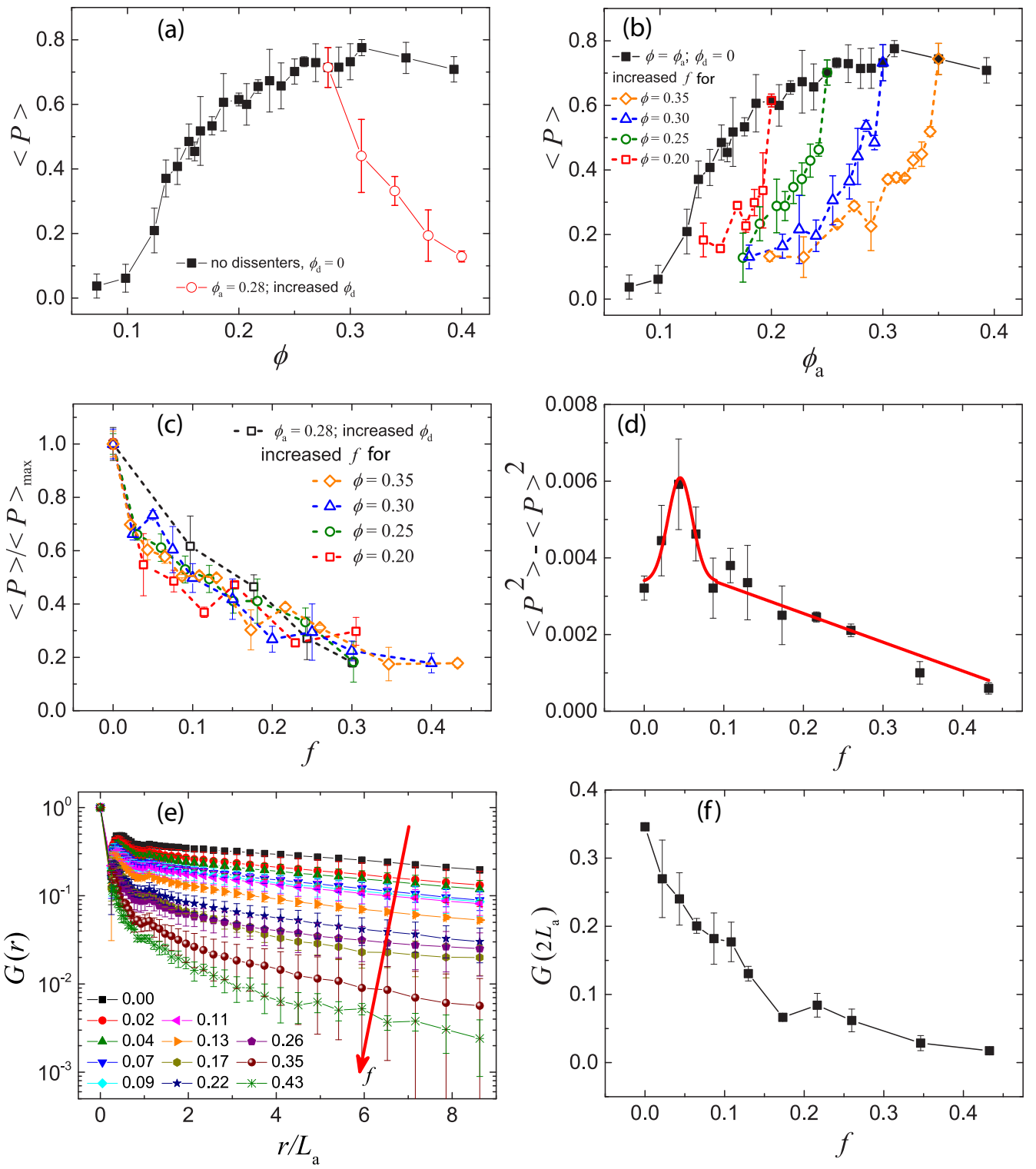

FIG. 3. The mixed system having aligners + dissenters. Error bars are calculated in the same way as in Fig. 2. (a) $\langle P \rangle$ vs ϕ is shown along with the plot from Fig. 2(b). $\phi = \phi_a + \phi_d$, where ϕ_a is the aligners' area fraction and ϕ_d is the dissenters' area fraction. (b) For four different fixed ϕ, $\langle P \rangle$ vs ϕ_a plots along with the plot from Fig. 2(b). The dissenter fraction $f = \phi_d/\phi$ was increased until the disordered state was reached. (c) $\langle P \rangle$ normalized with respect to the maxima are plotted vs f for all the mixed systems. (d) For $\phi = 0.35$, the variance of P in the steady state is plotted vs f. The red curve is the guide to the eyes, indicating a maximum near $f = 0.05$. (e) For $\phi = 0.35$, $G(r)$ vs r/L_a for different f are shown, without including the dissenters in the calculation. The red arrow is towards increasing f. (f) For $\phi = 0.35$, the value of $G(r)$ at $r = 2L_a$ is plotted vs f.

to follow the dynamics in time. The presence of dissenters disrupts the flocking [Fig. 3(a)], and the system shows reduced order parameter $\langle P\rangle$ with increasing ϕ (as we increase ϕ_d) (Supplemental Material [18], Movie S9). All error bars in Fig. 3 are the standard deviations over three repeated experiments. At a higher ϕ_d, it shows completely disordered motion (Supplemental Material [18], Movie S10). We note that the mixed system phase segregates at the high value of ϕ ($\gtrsim$0.58) and shows spatially restricted motion of the particles for $\phi \gtrsim 0.70$.

Now we keep the total ϕ fixed and increase the dissenters' fraction in the system ($f = \phi_d/\phi$) by substituting some aligners with dissenters in the system (Supplemental Material [18], Movies S11 and S12). In Fig. 3(b), we plot $\langle P\rangle$ vs ϕ_a with increasing f for different fixed values of ϕ until the system shows the completely disordered state. Black solid squares represent the same data as in Fig. 2(b), where we have $\phi_a = \phi$ as $\phi_d = 0$. Compared to the system with pure aligners, the crossover from ordered to disordered state happens at higher values of ϕ_a (depending on starting ϕ), implying that the effect of the dissenters is much stronger than that of simply diluting the system. To quantify these effects in terms of the fraction of dissenter particles f, we plot normalized $\langle P\rangle$ vs f in Fig. 3(c) which shows the collapse of all the data sets. We expect that the data collapse may be better with a much larger system size. The normalized order parameter $\langle P\rangle/\langle P\rangle_{max}$ decreases continuously from 1 and reaches the completely disordered state nearly at $f \sim 0.3$. Figure 3(c) suggests that the relative suppression of flocking by dissenters is independent of the area fraction of aligners.

The variance of the steady-state order parameter would be proportional to the susceptibility if this was an equilibrium system, and is in any case a measure of the magnitude of fluctuations. In the simulation study on the mixed aligner-dissenter system, Yllanes *et al.* [1] have shown that the variance shows a maximum at a dissenters' fraction where the order parameter reduces to ∼0.5 of its maximum value, indicative of an underlying phase transition in the infinite-size limit. We were curious to see if the variance of P exhibits such nonmonotonic behavior with respect to f. Figure 3(d) plots the variance of P as a function of f calculated considering the fluctuations observed in the steady state for $\phi = 0.35$, showing a peak at $f \sim 0.05$ where the order parameter is close to $0.5\langle P\rangle_{max}$, similar to the simulation results (see Fig. 3 of Ref. [1]). Here we may add a word of caution that the crossover point extracted from our data is only indicative due to finite-size effects.

It is also interesting to look at the mixed systems without including the contributions of dissenters in calculating $\langle P\rangle$, $G(r)$, etc. We have estimated separately contributions of aligners and dissenters in the normalized $\langle P\rangle$ vs f for $\phi = 0.35$ and observed negligible contributions of dissenters [Supplemental Material [18], Fig. S5(a)]. Also, the variance of P vs f considering only aligners [Supplemental Material [18], Fig. S5(b)] shows reduced values but still retains the maxima close to $f = 0.05$ as in Fig. 3(d). The negligible contribution of dissenters in the normalized $\langle P\rangle$ and variance is expected as they do not contribute to the collective behavior.

Next, we quantify the particle-level interactions in the mixed systems. For $\phi = 0.35$, in Figs. 3(e) and 3(f), we plot

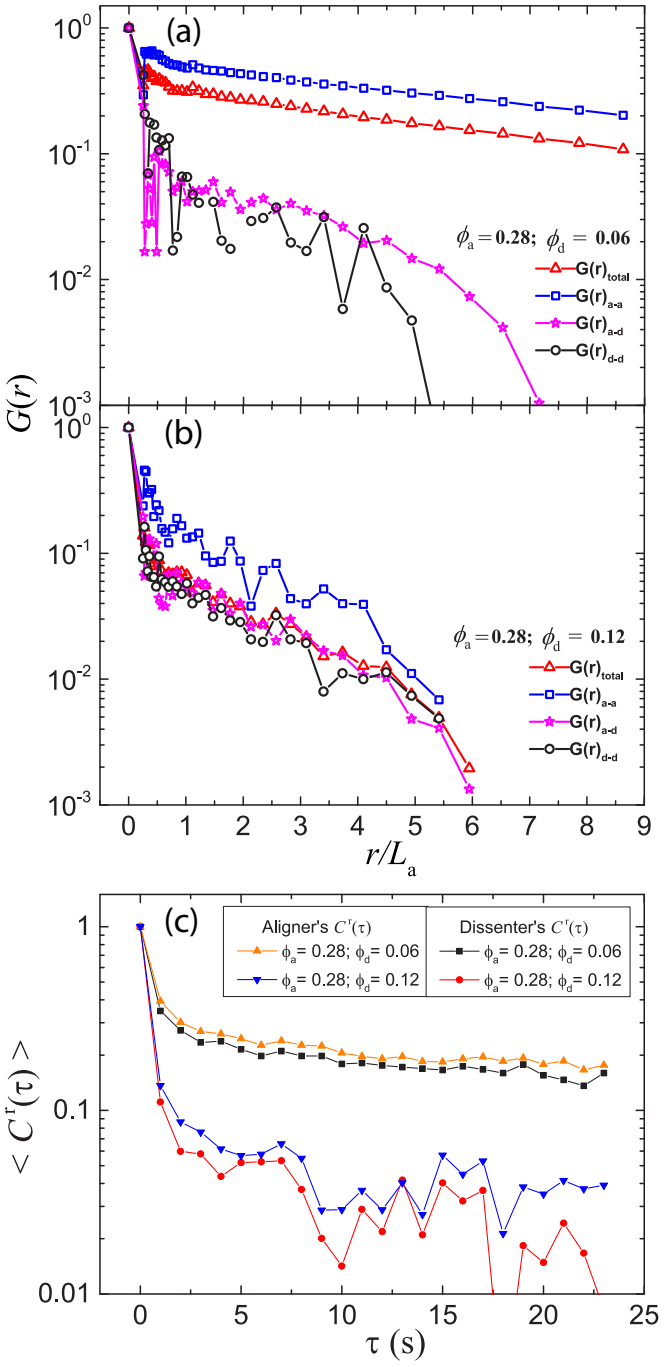

FIG. 4. (a) For the mixed systems, $G(r)$ vs r/L_a considering aligner-aligner (a-a), aligner-dissenter (a-d), and dissenter-dissenter (d-d) pairs separately and together for $\phi_a = 0.28$ and $\phi_d = 0.06$ are plotted. (b) Similar plots for $\phi_a = 0.28$ and $\phi_d = 0.12$ are shown. (c) $\langle C^r(\tau)\rangle$ vs τ is plotted by averaging separately over all aligners and over all dissenters, for the systems as in panels (a) and (b).

$G(r)$ vs r/L_a and $G(\text{at } r = 2L_a)$ vs f considering only aligners, without taking into account the contribution of dissenters. The plot shows a monotonic evolution from a highly correlated state to a low correlated state. When a small fraction of dissenters is present, the system can retain some order. With a high dissenters fraction, $G(r)$ falls rapidly with r/L_a to a low value showing negligible correlation between aligners.

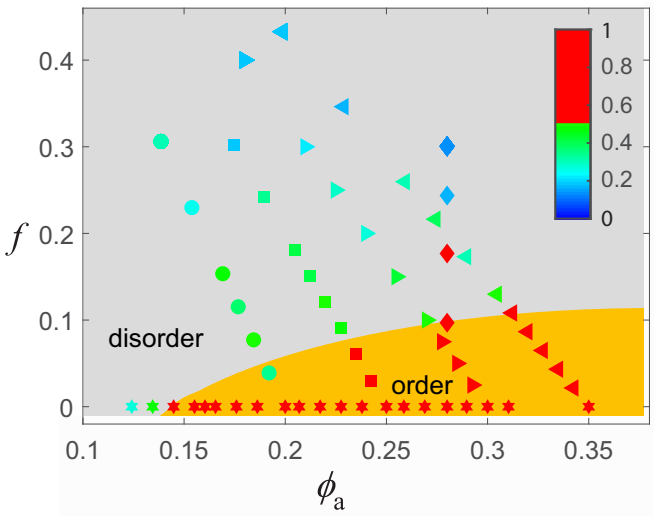

FIG. 5. The flocking phase diagram in the f-ϕ_a plane, considering data sets of Figs. 2 and 3, represented by different symbols. Color bars represent $\langle P\rangle/\langle P\rangle_{max}$ value. The order region and the disorder region are indicated by considering the crossover value $\langle P\rangle/\langle P\rangle_{max} \sim 0.5$.

The aligner-dissenter and the dissenter-dissenter pairs always show low orientational correlation even when the system shows flocking with high $\langle P\rangle$ at low f [Figs. 4(a) and 4(b)]. The dissenters are nonaligning agents which introduce rotational noise in the system. At a low fraction of the dissenters (e.g., $\phi_a = 0.28$ and $\phi_d = 0.06$), the aligners induce the dissenters to develop finite rotational autocorrelation [Fig. 4(c)]. At high f, the rotational autocorrelation of the aligners as well as the dissenters is highly reduced, thus disrupting the flocked state. By combining the observations shown in Figs. 2(b), 3(a), and 3(b), the phase diagram thus constructed of this flocking ordered to isotropic disordered transition is shown in Fig. 5. Here we take $\langle P\rangle/\langle P\rangle_{max} \sim 0.5$ to mark the boundary between order and disorder regions.

IV. CONCLUSIONS

In summary, our dry active granular system with two-step-tapered polar rods shows flocking in a wide range of the area fraction without any intervening medium. The order parameter varies smoothly around $\phi = 0.12$ due to finite system size which would be discontinuous in the larger system sizes as shown in the simulations [25]. Orientational correlations grow as the system approaches a threshold area fraction. We experimentally realize motile "dissenters" in the form of one-step-tapered polar particles that move in a fashion much more noisy than that of the two-step-tapered particles. To follow the transient behavior of the system during flocked to deflocking transition in the presence of dissenters, one has to pause the shaker after flock formation and replace some aligners in random places by dissenters, keeping all positions and directions unchanged, and then run the shaker to follow the dynamics in, time which is a very laborious task. Rather, we mix and disperse them to follow the system in the steady state. The effect of the dissenters is much stronger than that of simply diluting the system and it depends only on the ordering in the system, not on the aligners' area fractions. We have shown that the high rotational noise of the dissenters decorrelates all three types of orientational correlations (aligner-aligner, aligner-dissenter, and dissenter-dissenter) and disrupts the flocking of the active granular matter. The peak in the variance of the system's order parameter at $f \sim 0.05$ is associated with the finite-size crossover from an ordered to a disordered state. Our experimental results can be visualized in terms of real-life examples. For example, flocking is observed in animal groups having a small fraction of baby animals along with the adults, whereas the flocking is absent with a large fraction of baby animals. Another situation where deflocking can be desirable is the motion of a crowd in high-risk situations where a large number of dissenters do not allow collective motion. It will be interesting to study the effects of static obstacles on the flocking of the aligners.

ACKNOWLEDGMENTS

We thank Professor Sriram Ramaswamy for critical reading of the manuscript. A.K.S. thanks the Department of Science and Technology, India, for support through a Year of Science Professorship. P.K.B. thanks the University Grants Commission, India, for a Senior Research Fellowship.

[1] D. Yllanes, M. Leoni, and M. C. Marchetti, New J. Phys. **19**, 103026 (2017).
[2] O. Chepizhko, E. G. Altmann, and F. Peruani, Phys. Rev. Lett. **110**, 238101 (2013).
[3] A. Berdahl, C. J. Torney, C. C. Ioannou, J. J. Faria, and I. D. Couzin, Science **339**, 574 (2013).
[4] D. A. Quint and A. Gopinathan, Phys. Biol. **12**, 046008 (2015).
[5] E. Pinçe, S. K. P. Velu, A. Callegari, P. Elahi, S. Gigan, G. Volpe, and G. Volpe, Nat. Commun. **7**, 10907 (2016).
[6] A. Morin, N. Desreumaux, J.-B. Caussin, and D. Bartolo, Nat. Phys. **13**, 63 (2017).
[7] Cs. Sándor, A. Libál, C. Reichhardt, and C. J. Olson Reichhardt, Phys. Rev. E **95**, 032606 (2017).
[8] C. J. O. Reichhardt and C. Reichhardt, Nat. Phys. **13**, 10 (2017).
[9] C. Reichhardt and C. J. O. Reichhardt, Phys. Rev. E **97**, 052613 (2018).
[10] R. Das, M. Kumar, and S. Mishra, Phys. Rev. E **98**, 060602(R) (2018).
[11] B.-q. Ai, F.-h. Meng, Y.-l. He, and X.-m. Zhang, Soft Matter **15**, 3443 (2019).
[12] V. Guttal and I. D. Couzin, Proc. Natl. Acad. Sci. USA **107**, 16172 (2010).
[13] I. D. Couzin, C. C. Ioannou, G. Demirel, T. Gross, C. J. Torney, A. Hartnett, L. Conradt, S. A. Levin, and N. E. Leonard, Science **334**, 1578 (2011).
[14] S. R. McCandlish, A. Baskaran, and M. F. Hagan, Soft Matter **8**, 2527 (2012).

[15] G. Baglietto, E. V. Albano, and J. Candia, Phys. A (Amsterdam, Neth.) **392**, 3240 (2013).
[16] G. Ariel, O. Rimer, and E. Ben-Jacob, J. Stat. Phys. **158**, 579 (2015).
[17] K. Copenhagen, D. A. Quint, and A. Gopinathan, Sci. Rep. **6**, 31808 (2016).
[18] See Supplemental Material at, http://link.aps.org/supplemental/10.1103/PhysRevE.101.052615, which includes legends to movies, setup calibration, image analysis, references, and supplemental figures.
[19] D. Yamada, T. Hondou, and M. Sano, Phys. Rev. E **67**, 040301(R) (2003).
[20] V. Narayan, S. Ramaswamy, and N. Menon, Science **317**, 105 (2007).
[21] N. Kumar, S. Ramaswamy, and A. K. Sood, Phys. Rev. Lett. **106**, 118001 (2011).
[22] N. Kumar, R. K. Gupta, H. Soni, S. Ramaswamy, and A. K. Sood, Phys. Rev. E **99**, 032605 (2019).
[23] J. Schindelin, I. Arganda-Carreras, E. Frise, V. Kaynig, M. Longair, T. Pietzsch, S. Preibisch, C. Rueden, S. Saalfeld *et al.*, Nat. Methods **9**, 676 (2012).
[24] N. Kumar, H. Soni, S. Ramaswamy, and A. K. Sood, Nat. Commun. **5**, 4688 (2014).
[25] H. Chaté and B. Mahault, arXiv:1906.05542.
[26] C. Reichhardt and C. J. O. Reichhardt, Soft Matter **10**, 7502 (2014).